JASMAC Conference of the Japan Society of Microgravity Application

OR2-4

PMMA ロッド上を伝播する対向流拡散火炎の消炎限界予測

Prediction of Extinction Limit for Opposed Flow Diffusion Flame Propagating on PMMA Rods

○戸田寛人 [1]，中谷辰爾 [1]，津江光洋 [1]
○**Hiroto TODA[1], Shinji NAKAYA[1], Mitsuhiro TSUE[1]**
1　東京大学，The University of Tokyo

1. Introduction

Fire safety is one of the most important issues in manned space activities. To prevent fire, the flammability of materials needs to be evaluated using specific test methods. The most widely used material test method is NASA-STD-6001B [1]. Although this evaluation test is conducted in a normal gravity environment, previous studies suggested that combustion characteristics under normal gravity were different from those under microgravity [2-4]. Since fire safety in partial gravity environments also needs to be guaranteed in Moon and Mars missions, it is necessary to understand the effects of gravity level on combustion behaviours of solid materials, and to update space fire safety standards.

In fire safety of manned space activity, the limiting oxygen concentration (LOC) is one of the important measures. Fujita et al. showed that LOC could be low in a microgravity environment without buoyancy flow in combustion experiments of low density polyethylene (LDPE), which is used as a sheathing material for electric wires [2]. For LOC prediction, Takahashi et al. developed a simple scale analysis of opposed flow diffusion flame propagation on a thermally thin polymethyl methacrylate (PMMA) sheet and derived an equation relating the Damköhler number and the dimensionless radiation loss coefficient [3,4]. Since buoyancy flow was not considered in the LOC prediction model proposed by Takahashi et al., it cannot be applied in a partial gravity environment. In addition, sheet samples were considered in this model. However, it is known that the thickness and the curvature of the material also have significant effects on LOC [5].

The objective of this study is to develop a model for predicting the LOC of opposed flow diffusion flame propagation on a PMMA rod under normal gravity and validate the model by comparing the predicted LOC with experimentally measured LOC.

2. Scale Analysis of opposed flow diffusion flame propagation on a solid rod

For a solid sample in an opposed flow, there are two dominant mechanisms of the extinction limit depending on the opposed flow velocity: blow off in a high velocity flow and radiative extinction in a low velocity flow. Takahashi et al. predicted the flammability limit of sheet samples from a balance of heat transports in preheat zone: heat conduction from the flame, radiation heat loss from the solid surface, and amounts of preheating to the unburned sample [3,4].

In this study, the extinction limit of opposed diffusion flame propagation on a solid rod is predicted using a scale analysis. Figure 1 shows a model of the flame propagation on a rod-shaped solid sample with a rod radius of r_s placed in an opposed flow. A balance equation, taking into account the curvature of the rod and buoyancy flow velocity, is

$$V_f \rho_s c_s A_s (T_v - T_\infty) + \int_0^{L_g} 2\pi r_s \varepsilon (1-\alpha_{abs}) \sigma \left(T(x)^4 - T_\infty{}^4\right) dx \sim \left(1 - \frac{1}{D_a}\right) \frac{2\pi\lambda_g}{\ln\left(\frac{L_g + r_s}{r_s}\right)} L_g (T_f - T_v), \quad (1)$$

where $V_f, \rho_s, c_s, A_s, T_f, T_v, T_\infty, L_g, \varepsilon, \alpha_{abs}, \sigma$, and λ_g indicate flame spread rate, solid density, specific heat of solid, rod cross-

sectional area, characteristic flame temperature, pyrolysis temperature, ambient temperature, gas-phase diffusion length scale, surface emissivity, absorption coefficient of gas, Stefan–Boltzmann constant, and gas-phase conductivity, respectively. The linear temperature distribution in preheat zone $T(x)$ is assumed with T_v at the upper end of the zone ($x = 0$) and T_∞ at the lower end of the zone ($x = L_g$).

In addition, axial heat conduction needs to be considered since the rod sample has a certain cross-sectional area in this study. Assuming that the temperature distribution is uniform on the cross section, the axial heat conduction $\dot{Q}_{cond,ax}$ is

$$\dot{Q}_{cond,ax} = \frac{A_s \lambda_s (T_v - T_\infty)}{L_g}, \tag{2}$$

where λ_s indicates solid thermal conductivity. By adding the heat conduction term to Eq. (1), it can be rewritten as follows:

$$V_f \rho_s c_s A_s (T_v - T_\infty) + \int_0^{L_g} 2\pi r_s \varepsilon (1 - \alpha_{abs}) \sigma \left(T(x)^4 - T_\infty{}^4\right) dx \sim \left(1 - \frac{1}{D_a}\right) \frac{2\pi \lambda_g}{\ln\left(\frac{L_g + r_s}{r_s}\right)} L_g (T_f - T_v) + \frac{A_s \lambda_s (T_v - T_\infty)}{L_g}. \tag{3}$$

When this is nondimensionalized using the method showed in Ref. 3), we obtain

$$\eta + R_{rad} + \frac{1}{D_a} = 1 + \Lambda_{cond,ax}, \tag{4}$$

where $R_{rad}, D_a,$ and $\Lambda_{cond,ax}$ indicate radiation loss number, Damköhler number, and axial heat conduction number, respectively. These are expressed as follows:

$$D_a = \frac{\alpha_g}{V_r{}^2} \rho_g Y_o A \exp\left(-\frac{E}{R T_f}\right), \tag{5}$$

$$R_{rad} = \frac{\varepsilon (1 - \alpha_{abs})}{\rho_g c_g V_r (T_f - T_v)} \left(\frac{T_v{}^5 - T_\infty{}^5}{5(T_v - T_\infty)} - T_\infty{}^4\right) \frac{r_s}{L_g} \ln\left(\frac{L_g + r_s}{r_s}\right), \tag{6}$$

$$\text{and } \Lambda_{cond,ax} = \frac{1}{2} \frac{\lambda_s}{\lambda_g} \frac{T_v - T_\infty}{T_f - T_v} \frac{r_s{}^2}{L_g{}^2} \ln\left(\frac{L_g + r_s}{r_s}\right), \tag{7}$$

where $V_r, \alpha_g, \rho_g, Y_o, A, E,$ and R indicate opposed flow velocity, thermal diffusivity of gas, gas density, oxygen mass fraction, pre-exponential factor, activation energy, and gas constant, respectively.

The opposed flow velocity V_r is defined as a sum of the flame spread rate V_f, forced flow velocity V_g, and buoyancy flow velocity V_b. In previous studies of the opposed diffusion flame propagation on sheet and rod samples, the buoyancy term in the momentum equation is assumed to be equal to the inertia term. Thus, the buoyancy flow velocity was obtained [6,7]. Therefore, V_r is calculated as follows:

$$V_r = V_f + V_g + V_b \sim V_g + V_b = V_g + \left[\frac{\alpha_g g (T_f - T_\infty)}{T_v}\right]^{\frac{1}{3}}, \tag{8}$$

where V_f is considered to be sufficiently lower than V_g and V_b.

The LOC is predicted from Eq. (4), where dimensionless flame spread rate η is equal to 0 (at flame extinction).

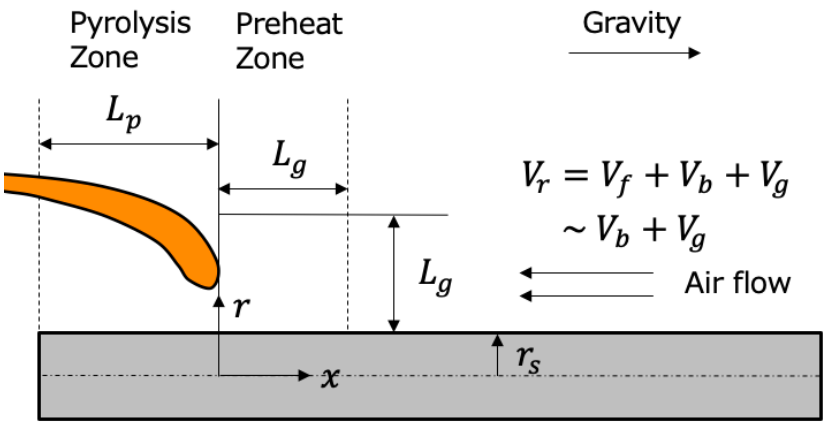

Fig. 1 Schematic diagram of opposed flow diffusion flame propagation on a solid rod

3. Experimental Apparatus

For validating Eq. (4), LOC was measured from flame propagation experiments in opposed flow using cast PMMA as a target sample. Figure 2 shows a schematic diagram of the experimental apparatus. Nitrogen and oxygen were supplied from the bottom of the combustion chamber (overall length = 300mm, inner diameter = 80mm) and flowed to the top. Nitrogen and oxygen flow rates were individually controlled by mass flow controllers (KOFLOC 8550MC). The PMMA sample was ignited by heating a nichrome wire at the tip of the rod. After confirming ignition, the power supply was cut off and the behaviour of the flame was recorded with a digital camera (Sony α6500 with a resolution of 1440 × 810 pixels at 120 frames per second).

Forced flow velocity and rod diameter were chosen as parameters in order to investigate the effect of sample curvature and opposed flow velocity. The forced flow velocities were set to 10, 20, 40, and 60 cm/s, and rod samples with diameters of 4, 6, and 10 mm were used. For these 12 experimental conditions, flame spread tests were conducted with different oxygen concentrations, and the LOC was identified by observing flame extinction limit.

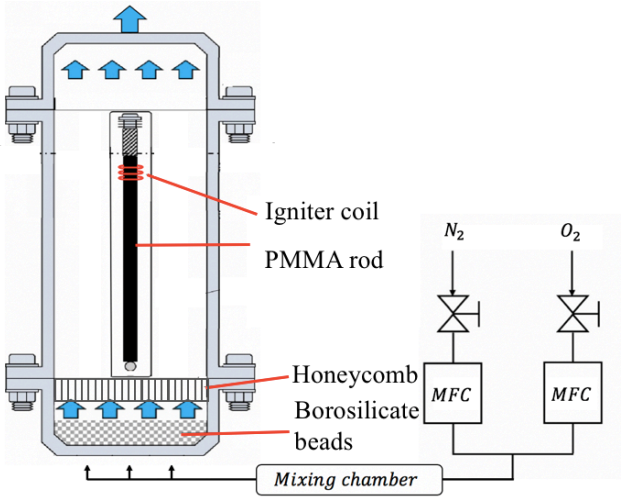

Fig. 2 Schematic diagram of combustion chamber and fluid system.

4. Results

First of all, LOC under each condition was measured from the flame spread experiments. Figure 3 shows scatter plots of flame propagation and extinction for opposed diffusion flame on PMMA rods with diameter = 4, 6, and 10 mm at the various oxygen concentration and flow velocity. For each diameter, the result showed that LOC increased with increasing the forced flow velocity. It seems that the effect of $1/D_a$ in Eq. (4) became larger as the flow velocity increases, and blow off was more likely to occur. Under the condition of high flow velocity ($V_g = 60cm/s$), LOC decreased with increasing the

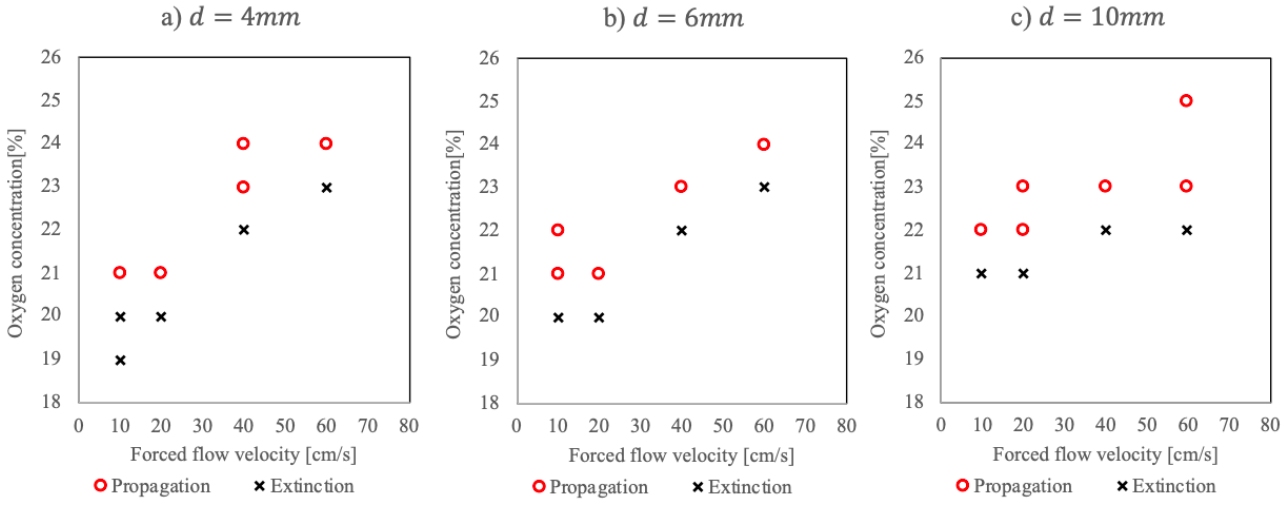

Fig. 3 Scatter plots of flame propagation and extinction for opposed diffusion flame on PMMA rods (rod diameter = a) 4mm, b) 6mm, and c) 10mm)

rod diameter. Under low flow velocity conditions, the radiative heat loss term becomes small, and blow off term and axial heat conduction term are dominant. Therefore, it seems that the sample with a larger cross-sectional area burns more easily due to the effect of $\Lambda_{cond,ax}$. On the other hand, under the condition of low flow velocity ($V_g = 10cm/s$), LOC increased with increasing the rod diameter. This mechanism is discussed at the latter part.

Next, LOC was predicted from Eq. (4). Properties of the PMMA for predicting LOC were given in Table 1. For quantitative evaluation, experimental constants B_1, B_2, B_3, and B_4 for $D_a, R_{rad}, \Lambda_{cond,ax}$, and V_r were introduced as follows:

$$D_a = B_1 \frac{\alpha_g}{{V_r}^2} \rho_g Y_o A exp\left(-\frac{E}{RT_f}\right), \tag{9}$$

$$R_{rad} = B_2 \frac{\varepsilon(1-\alpha_{abs})}{\rho_g c_g V_r (T_f - T_v)} \left(\frac{{T_v}^5 - {T_\infty}^5}{5(T_v - T_\infty)} - {T_\infty}^4\right) \frac{r_s}{L_g} \ln\left(\frac{L_g + r_s}{r_s}\right), \tag{10}$$

$$\Lambda_{cond,ax} = B_3 \frac{1}{2} \frac{\lambda_s}{\lambda_g} \frac{T_v - T_\infty}{T_f - T_v} \frac{{r_s}^2}{{L_g}^2} \ln\left(\frac{L_g + r_s}{r_s}\right), \tag{11}$$

$$\text{and } V_r = V_g + B_4 \left[\frac{\alpha_g g (T_f - T_\infty)}{T_v}\right]^{\frac{1}{3}}. \tag{12}$$

These four constants were determined by the experimental results under four conditions: $B_1 = 0.118, B_2 = 57.2, B_3 = 0.0709$, and $B_4 = 2.19$.

Figure 4 shows the results of LOC prediction using B_1, B_2, B_3, B_4, and Eq. (4). In Fig. 4, "Experiment" means the LOC measured by the experiments, and "Predicted" presents the LOC predicted from Eq. (4) with the four constants. For each diameter, the result showed that LOC increased with increasing the forced flow velocity. This showed a similar tendency to the experimental results. Also, predicted LOC decreased with increasing the rod diameter. It seems that the blow off term and axial heat conduction term are dominant due to the effect of buoyancy flow under normal gravity and the heat conduction term is high for large diameter sample. It will be necessary to conduct flame spread experiments in which the radiation loss term is dominant and investigate the effect of rod curvature in a microgravity environment with low buoyancy flow velocity. In addition, under low flow velocity conditions, experiment LOC increased with increasing the rod diameter and there was a large difference between the experiment LOC and the predicted LOC for large diameter

Table 1 Properties of PMMA [4)]

Property	Value	Units
Solid density, ρ_s	1190	kg/m^3
Solid specific heat, c_s	1.465	$kJ/Kg \cdot K$
Solid thermal conductivity, λ_s	0.19	$W/m \cdot K$
Pyrolysis temperature, T_v	670	K
Pre-exponential factor, A	1.36×10^9	$m^3/kg \cdot s$
Activation energy, E	1.50×10^5	J/mol
Surface emissivity, ε	1.0	-

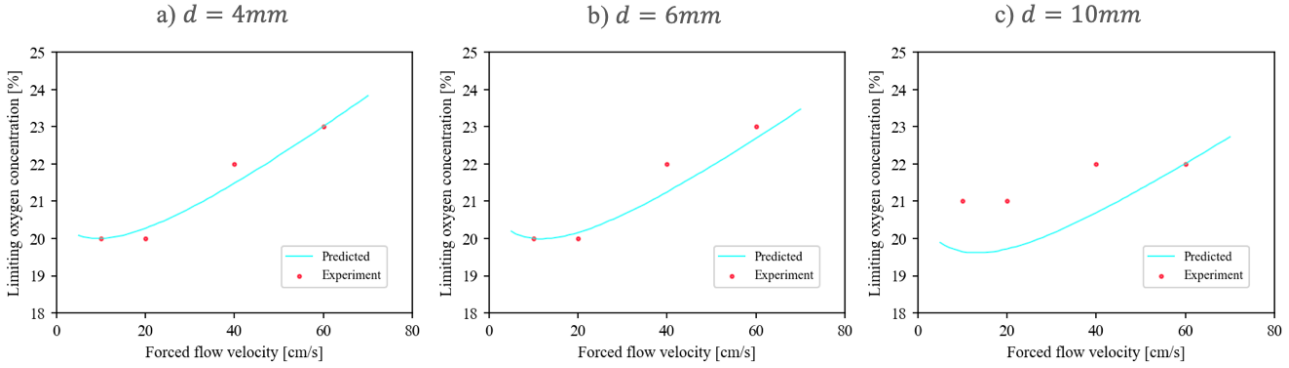

Fig. 4 Scatter plots of LOC measured by flame spread experiments and LOC predicted from Eq. (4) (rod diameter = a) 4mm, b) 6mm, and c) 10mm)

sample ($d = 10mm$). Since the inlet oxygen flow rate was controlled by the mass flow controllers, the buoyancy flow velocity seemed to be higher than the inlet flow velocity, resulting in a recirculation flow in the combustor. Under low flow velocity conditions, the mass loss rate of the rod becomes larger with increasing the diameter, leading to the low oxygen concentration in the combustor due to the combustion-gas recirculation. It seems that under low flow velocity conditions, the sample with larger rod diameter is less flammable due to this mechanism. We are going to validate this effect by conducting experiments using a larger volume combustor and velocity measurements.

5. Conclusion

A model for predicting the extinction limit of opposed diffusion flame propagation on a material rod sample was proposed. In addition to the three heat terms (heat conduction from the flame, radiation heat loss from the solid surface, and amounts of preheating to the unburned sample), which were considered in a predict model for sheet sample, axial heat conduction term was also considered. Using PMMA as a target sample, the LOC measured from the experimental results was compared with the LOC predicted from the model. The results showed that the blow off term and axial heat conduction term are dominant under normal gravity environment, and the sample with larger rod diameter is more flammable. For increasing the accuracy of the model, more experimental results are necessary. Farther experiments will be conducted.

Acknowledgement

This study was financially supported by Japan Society for the Promotion of Science (JSPS) KAKENHI (Grant-in-Aid for Challenging Research Exploratory, 21K18775). Also, it is being carried out under a feasibility study theme using Kibo "Evaluation of Flammability of Solid Materials in Space Habitation" (FLARE2). We are grateful to JAXA and other related organizations for their cooperation in promoting this study.

References

1) NASA-STD-6001 B: Flammability, offgassing, and compatibility requirements and test procedures (2011).
2) O. Fujita: Proceedings of the Combustion Institute **35** (2015) 2487–2502.
3) S. Takahashi, M.A.F. bin Borhan, K. Terashima, A. Hosogai, and Y. Kobayashi: Proceedings of the Combustion Institute **37** (2019) 4257–4265
4) S. Takahashi: Int. J. Microgravity Sci. Appl. **32** (4) 2015, 320403
5) Y. Konno, N. Hashimoto, and O. Fujita: Proceedings of the Combustion Institute **37** (2019) 3817–3824
6) Maria Thomsen, Carlos Fernandez-Pello, Xinyan Huang, Sandra L. Olson, and Paul V. Ferkul: Fire Safety Journal **110** (2019) 102903
7) Subrata Bhattacharjee and Luca Carmignani: Proceedings of the Combustion Institute **38** (2021) 4795–4803